Journal of Applied Physics

Solid-state electrochemical redox control of the optoelectronic properties for $SrFeO_x$ thin films

Cite as: J. Appl. Phys. **129**, 215303 (2021); https://doi.org/10.1063/5.0053939
Submitted: 13 April 2021 . Accepted: 15 May 2021 . Published Online: 02 June 2021

Qian Yang, Hai Jun Cho, Hyoungjeen Jeen, Hiromichi Ohta, et al.

Journal of Applied Physics ARTICLE scitation.org/journal/jap

Solid-state electrochemical redox control of the optoelectronic properties for $SrFeO_x$ thin films

Cite as: J. Appl. Phys. **129**, 215303 (2021); doi: 10.1063/5.0053939
Submitted: 13 April 2021 · Accepted: 15 May 2021 ·
Published Online: 2 June 2021

View Online Export Citation CrossMark

Qian Yang,[1,a)] Hai Jun Cho,[1,2] Hyoungjeen Jeen,[3] and Hiromichi Ohta[1,2,a)]

AFFILIATIONS

[1]Graduate School of Information Science and Technology, Hokkaido University, N14W9, Kita, Sapporo 060-0814, Japan
[2]Research Institute for Electronic Science, Hokkaido University, N20W10, Kita, Sapporo 001-0020, Japan
[3]Department of Physics, Pusan National University, Busan 46241, South Korea

[a)]**Authors to whom correspondence should be addressed:** yangqian@eis.hokudai.ac.jp and hiromichi.ohta@es.hokudai.ac.jp

ABSTRACT

By utilizing redox reactions, the physical properties of several transition metal oxides can be drastically changed, which is useful for developing multifunctional memory devices. Strontium iron oxide ($SrFeO_x$), which exhibits a clear phase transition from antiferromagnetic insulator ($x = 2.5$) to helimagnetic metal ($x = 3$), is a good candidate for the active material in multifunctional memory devices. However, practical applications using previous demonstrations of redox reactions in $SrFeO_x$ are limited by the use of a liquid electrolyte due to the leakage problem. Here, we demonstrate solid-state electrochemical redox reaction in $SrFeO_x$ using a yttria-stabilized zirconia (YSZ) single-crystal substrate as the solid electrolyte. We fabricated the $SrFeO_{2.5}$ film on the YSZ substrate and the applied electric current using Au electrodes. The phase gradually changed from $SrFeO_{2.5}$ to $SrFeO_{2.5+x}$ and $SrFeO_{3-x}$. The color of the film changed from yellowish-transparent to dark brown. Although the as-grown $SrFeO_{2.5}$ film showed high resistivity ($\rho > 10^1\,\Omega\,cm$), the ρ dramatically decreased ($\sim 10^{-2}\,\Omega\,cm$) with increasing the applied charge density. Simultaneously, the thermopower greatly decreased from $\sim +200$ to $\sim -10\,\mu V\,K^{-1}$. The present results would provide a design concept for future $SrFeO_x$-based solid-state multifunctional memory devices.

I. INTRODUCTION

Nowadays, advanced memory devices that store multiple information are in high demand due to the significant increase in the sheer volume of information in next generation devices. In this regard, materials that can be switched electrically between electrically insulating and conducting state are promising as the active materials for advanced electrical memory devices.[1,2] With changing the oxygen content, several transition metal oxides (TMOs)[3–7] exhibit topotactic phase transition between brownmillerite (BM) and perovskite (PV). BM and PV phases usually exhibit completely different physical properties due to the difference in the valence state of TM ions.[8] Since the electrical, magnetic, and optical properties of such TMOs can be modulated by appropriate redox reactions, these materials are suitable for the active material of multifunctional memory devices.[9–14] For example, strontium cobalt oxide is known as the oxygen sponge and exhibits reversible BM to PV transition controlled by electrochemical redox reactions.[11,15]

In this study, we focus on strontium iron oxide ($SrFeO_x$). $SrFeO_x$ exhibits a clear phase transition from orthorhombic BM antiferromagnetic insulator ($x = 2.5$, Fe^{3+}) to cubic PV helimagnetic metal ($x = 3$, Fe^{4+})[16,17] at different oxide ion (O^{2-}) concentrations.[18–20] In 2017, Khare *et al.*[21] realized the phase transformation of $SrFeO_x$ epitaxial films from $SrFeO_{2.5}$ to $SrFeO_3$ by post-annealing in O_2 atmosphere. In 2019, Saleem *et al.*[22] demonstrated the electrochemical topotactic phase transition of $SrFeO_x$ epitaxial films using ionic liquid as the electrolyte. However, these examples of phase transition reactions involve intensive chemical reaction at extreme conditions such as high temperature or the usage of liquid electrolyte with leakage risks, which cannot be utilized in practical applications. For overcoming this issue, all solid structure is considered prominent.

In our previous study, we successfully realized the electrochemical oxidation reaction of $SrCoO_x$ using yttria-stabilized zirconia (YSZ) as the solid-state electrolyte.[15] Here, we fabricated $SrFeO_x$ epitaxial films on the YSZ single-crystal substrate and performed electrochemical redox reaction. As a result, insulator ($SrFeO_{2.5}$) to metal ($SrFeO_{3-x}$) transition occurred with a topotactic redox reaction, changing the optical and electrical properties.

The present results would provide a design concept for future $SrFeO_x$-based solid-state multifunctional memory devices.

II. EXPERIMENTAL DETAILS

A. Sample preparation

$SrFeO_x$ films were fabricated by pulsed laser deposition (PLD) technique. First, ~10-nm-thick GDC (10 mol. % Gd-doped CeO_2) was heteroepitaxially grown on a yttria-stabilized zirconia (YSZ, $10 \times 10 \times 0.5$ mm^3, double side mirror polished, Crystal Base Co.) substrate at 750 °C in an oxygen atmosphere (3 Pa) by irradiating focused KrF excimer laser pulses ($\lambda = 248$ nm, fluence ~1.2 J cm^{-2} pulse^{-1}, repetition rate = 10 Hz) on a ceramic target of GDC. GDC is a well-known oxide ion conducting electrolyte, which we used as the buffer layer to prevent undesired chemical reactions during the electrochemical redox treatment at 300 °C. Subsequently, ~45–64-nm-thick $SrFeO_{2.5}$ film was heteroepitaxially grown on the GDC film at 750 °C in an oxygen atmosphere (1×10^{-3} Pa). The laser fluence was ~1.6 J cm^{-2} pulse^{-1}. After the bilayer film growth, the sample was cooled down to room temperature in the PLD chamber in an oxygen atmosphere (1×10^{-3} Pa).

B. Electrochemical oxidation treatment

Electrochemical oxidation of the resultant $SrFeO_x$ films was performed at 300 °C in air. First, a porous Au electrode was sputtered on the back surface of the YSZ substrate using DC sputtering at room temperature. Then, the film surface was mechanically pressed on an Au foil. Using the Au electrodes, we applied current under a constant voltage of −5 V. The applied electron density (Q) was calculated as $Q = (\int I(t) \cdot dt)/(V \cdot e)$, where $I(t)$ is the current at the time t, V is the volume of the $SrFeO_x$ film, and e is the electron charge, respectively. The ideal Q for converting $SrFeO_{2.5}$ into $SrFeO_3$ is 1.65×10^{22} cm^{-3}. After applying the current, the sample was immediately cooled down to room temperature.

C. Crystallographic analyses

The film thickness, bulk density, crystallographic phase, and orientation were analyzed using a high-resolution x-ray diffractometer with Cu Kα_1 ($\lambda = 1.54059$ Å) radiation (ATX-G, Rigaku Co.). X-ray reflectivity, out-of-plane Bragg diffraction pattern, rocking curve, and reciprocal space mapping of the samples were measured at room temperature. Surface morphology of the $SrFeO_x$ films were observed using an atomic force microscopy (AFM, Nanocute, Hitachi Hi-Tech Co.) at room temperature.

D. Electrical property measurements

The electrical resistivity of the $SrFeO_x$ films was measured by a dc four-probe method with van der Pauw electrode configuration. A small amount of In–Ga alloys was used as the contact electrode. Thermopower values were measured by conventional steady state method at room temperature by introducing temperature differences in the films.[23]

E. Optical transmission spectra

After mechanically removing the sputtered Au film, we measured the optical transmission spectrum of the samples using a UV–VIS–NIR spectrometer (SolidSpec-3700, Shimadzu Co.).

III. RESULTS AND DISCUSSION

The $SrFeO_{2.5}$ film was heteroepitaxially grown on a (001) oriented yttria-stabilized zirconia (YSZ) single-crystal substrate with 6-nm-thick 10 mol. % Gd-doped CeO_2 (GDC). The YSZ substrate was utilized as the oxide ion conducting electrolyte (conductivity:

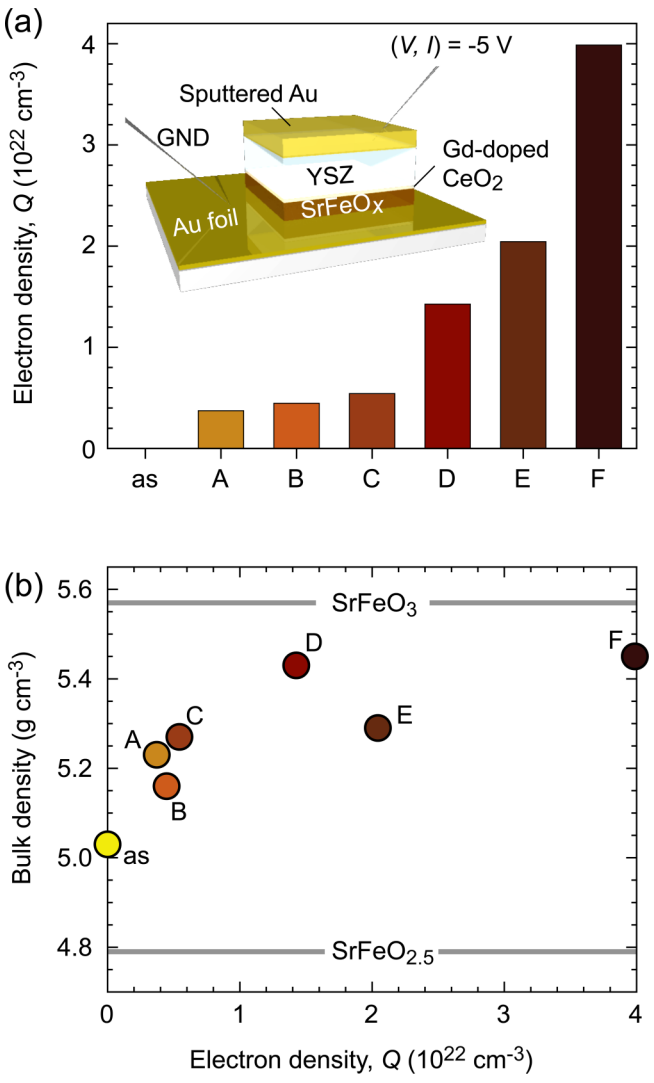

FIG. 1. Electrochemical oxidation of $SrFeO_x$ films. (a) $SrFeO_x$ film samples oxidized by applying varied electron densities. The inset shows the schematic experimental setup of the electrochemical oxidation. (b) Bulk density of the $SrFeO_x$ films vs electron density (Q). The bulk density gradually increases with Q.

$\sim 10^{-6}$ S cm^{-1} at 300 °C[24]), and the thickness of sputtered porous Au film on the back side of the YSZ substrate was 55 nm. The $SrFeO_{2.5}$/GDC/YSZ/Au multilayer structure sample was put on an Au foil and heated at 300 °C in air as shown in the inset of Fig. 1(a). It should be noted that the $SrFeO_x$ film surface was kept clean after the electrochemical oxidation. A current was applied under a negative voltage (−5 V) to oxidize the $SrFeO_x$ epitaxial films to various oxidation states. The samples with different applied electron densities were marked as A (0.15×10^{22} cm^{-3}), B (0.37×10^{22} cm^{-3}), C (0.54×10^{22} cm^{-3}), D (1.43×10^{22} cm^{-3}), E (2.04×10^{22} cm^{-3}), and F (3.99×10^{22} cm^{-3}), respectively (see Fig. S1 in the supplementary material for more details).

After the oxidation treatment, the bulk density and the thickness were measured by the x-ray reflectivity (Fig. S2 in the supplementary material). Bulk density of the as-grown $SrFeO_x$ film was ∼5.0 g cm^{-3}, which is slightly greater than that of $SrFeO_{2.5}$

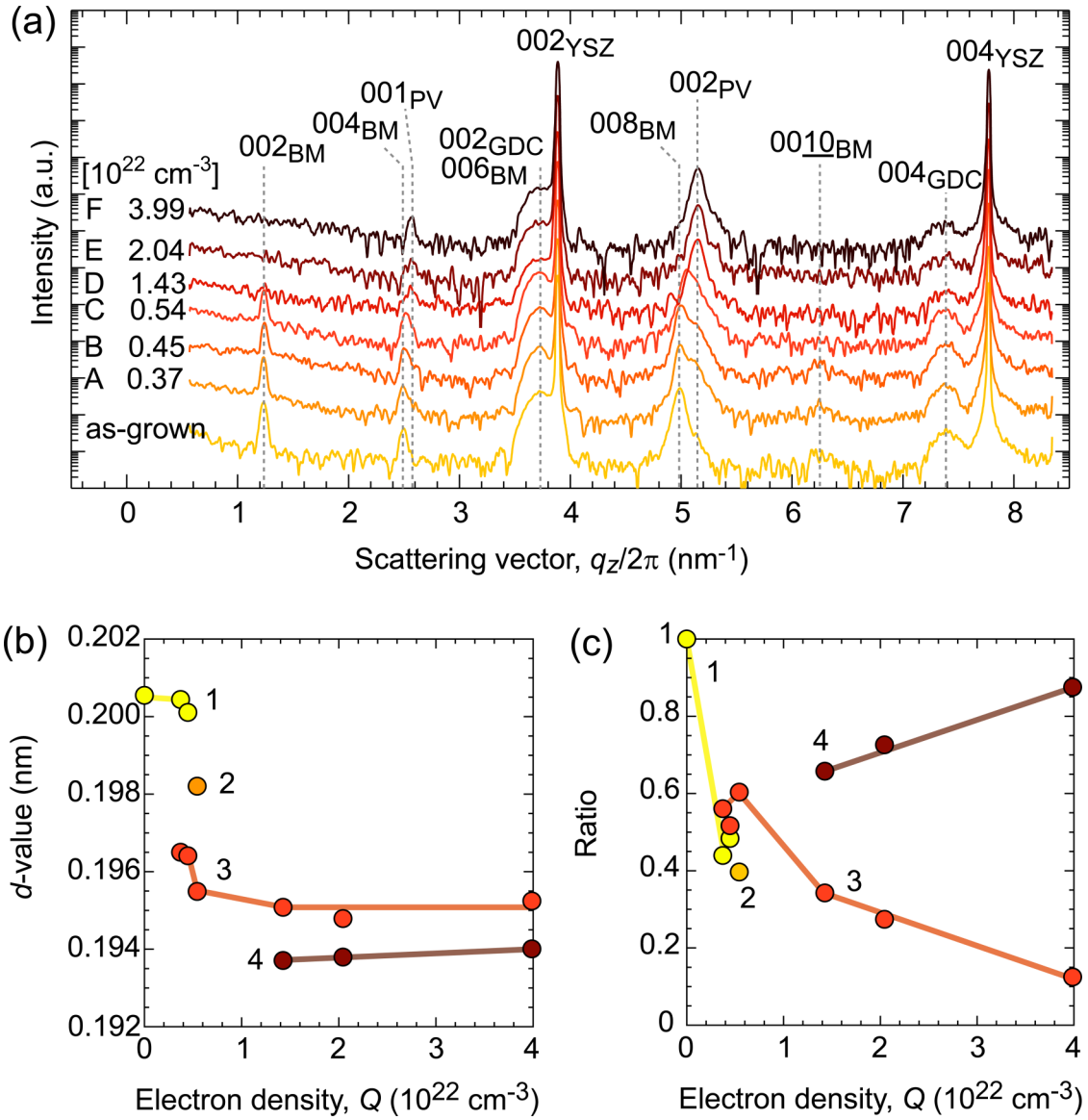

FIG. 2. Crystalline phases of the resultant $SrFeO_x$ films. (a) Out-of-plane XRD patterns. BM, Brownmillerite and PV, perovskite. With increasing the electron density Q, the BM phase changes into the PV phase. (b) Changes in the *d*-value of 008BM or 002PV as a function of Q. 1: $SrFeO_{2.5}$, 2 and 3: $SrFeO_{2.5+x}$, and 4: $SrFeO_{3-x}$. (c) Change in the volume ratio of the phases as a function of Q.

(~4.8 g cm^{-3}), and it gradually increased with Q [Fig. 1(b)]. The bulk density of sample F (3.99×10^{22} cm^{-3}) was ~5.5 g cm^{-3}, which is close to that of $SrFeO_3$.

Then, we analyzed the crystalline phase of the resultant $SrFeO_x$ films. Only intense diffraction peaks of 00l BM-$SrFeO_{2.5}$ are seen in the out-of-plane XRD pattern of the as-grown film [Fig. 2(a)] together with 00l GDC/00l YSZ, indicating the strong c-axis orientation of the BM-$SrFeO_{2.5}$. Upon reaching $Q > 1.43 \times 10^{22}$ cm^{-3}, the diffraction peak of 002 BM disappeared, indicating a phase transition occurred. In addition, the diffraction peak around $q_z/2\pi = 5$ nm^{-1} shifted to the right (higher $q_z/2\pi$) with increasing Q. In order to clarify the origin of this peak shift, the diffraction peaks were deconvoluted using Gaussian functions (Fig. S3 in the supplementary material). With increasing Q, the phase changed step-by-step from $SrFeO_{2.5}$ to $SrFeO_{2.5+x}$ and PV $SrFeO_{3-x}$.

To confirm the crystalline phases, the interplanar distances (d-values) were extracted from the magnified XRD patterns (Fig. S3 in the supplementary material). The d-value changed step-by-step from 0.205 to 0.198, 0.1955, and 0.194 nm, these values were

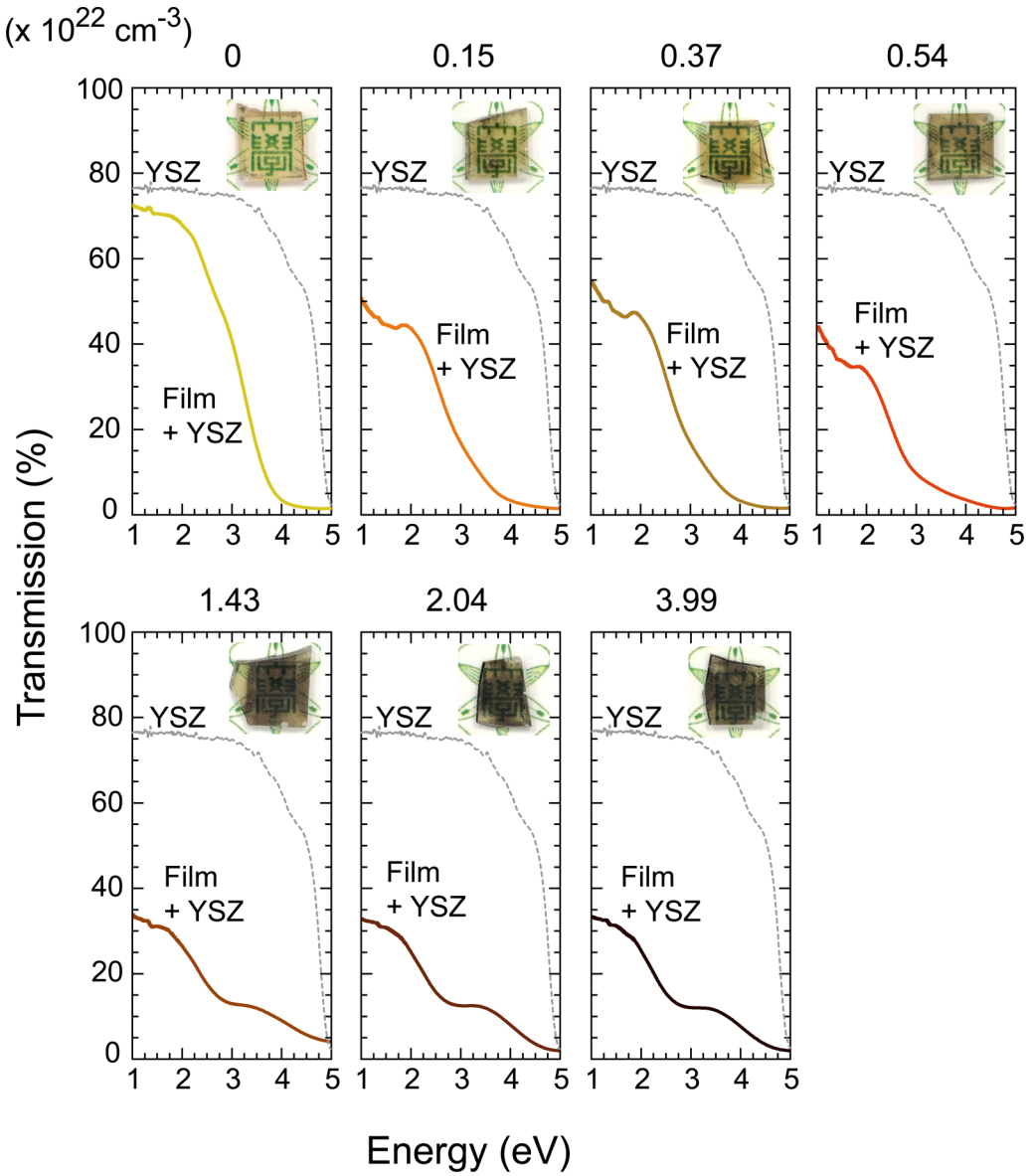

FIG. 3. Optical transmission spectra of the resultant $SrFeO_x$ films on the YSZ substrate. Transmission spectrum of the YSZ substrate is also plotted for comparison.

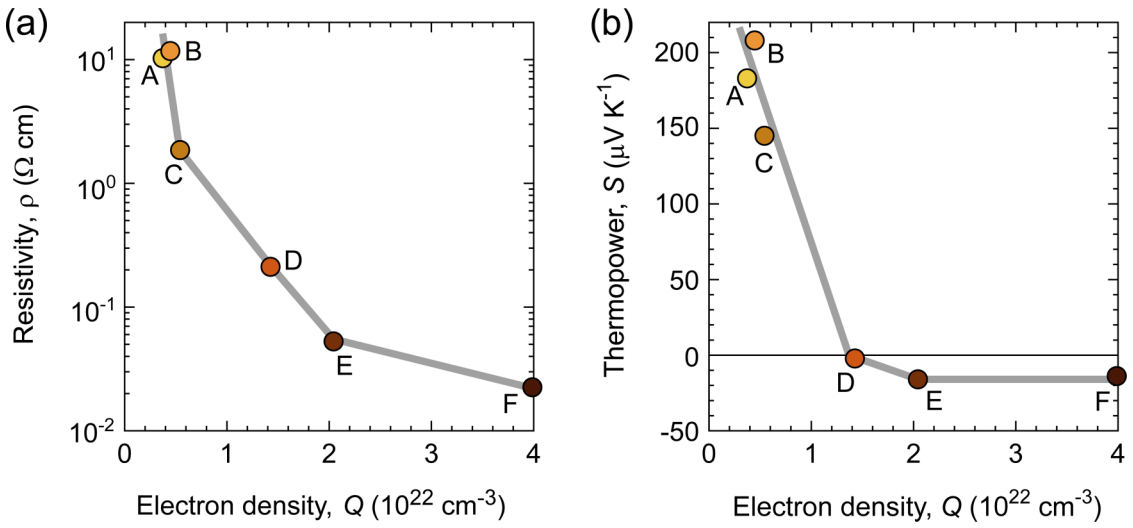

FIG. 4. Electrical properties of the resultant $SrFeO_x$ films. (a) Resistivity and (b) thermopower. Although the as-grown $SrFeO_{2.5}$ film showed high resistivity ($\rho > 10^1\ \Omega$ cm), the ρ dramatically decreased ($\sim 10^{-2}\ \Omega$ cm) with increasing the applied charge density. Simultaneously, the thermopower decreased dramatically from ~+200 to $\sim -10\ \mu V\ K^{-1}$.

similar to those of $SrFeO_{2.5}$, $SrFeO_{2.75}$, $SrFeO_{2.875}$, and $SrFeO_3$, respectively. Furthermore, we analyzed the peak area ratio [Fig. 2(c)]. With increasing Q, the as-grown $SrFeO_{2.5}$ developed into phase $SrFeO_{2.5+x}$. Furthermore, the volume of $SrFeO_{2.5+x}$ decreased but that of $SrFeO_{3-x}$ increased along the increasing of Q.

Then, we observed the surface morphology of the resultant films using atomic force microscopy (AFM) (Fig. S4 in the supplementary material). Several ten-nanometer-sized grain structures were observed in all cases. When $Q > 1.43 \times 10^{22}\ cm^{-3}$, square-shaped morphologies were observed, most likely due to the change of the bulk density. The root mean square roughness was ~0.2 nm, which almost did not change after the oxidation treatment.

Figure 3 summarizes the optical transmission spectra of the films. The as-grown film was yellowish-transparent, and the optical transmission at 2 eV was ~70% due to the high optical reflection of the YSZ substrate (~25%). The optical bandgap of the as-grown film is ~2 eV, consistent with the reported value. A slight change in the curvature around 2.7 eV is observed, indicating charge transfer absorption from O 2p to Fe 3d in BM-$SrFeO_{2.5}$.[21,25] With increasing Q, the color changed to dark brown, and the overall optical transmission gradually reduced. After oxidation at $Q = 3.99 \times 10^{22}\ cm^{-3}$, the optical transmission at 2 eV decreased to ~30%. Two absorptions, located ~1.5 and ~2.5 eV, are observed in oxidized $SrFeO_x$ with increasing Q. These absorption peaks have been assigned as γ (charge transfer from O 2p to Fe 3d octahedral t_{2g}) and δ (charge transfer from O 2p to Fe 3d octahedral e_g) of perovskite $SrFeO_3$, respectively.[21, 25] Furthermore, similar change in the oxidation state of Co from +3 to +4 has been observed in the $SrCoO_x$ films deposited under varying oxygen pressures.[26] These results clearly indicate that the oxidation state of Fe increased from +3 to +4 with increasing Q. It should be noted that these change in the optical transmission is reversible; the transmission at 550 nm in the wavelength changed from 65% (reduced) to 6% (oxidized) repeatedly (Fig. S5 in the supplementary material).

Finally, we measured the electrical properties of the films (Fig. 4). The electrical resistivity of the as-grown sample was too high to be measured using the dc setup. After the oxidation treatment, the resistivity significantly decreased from $\sim 10^1$ to $\sim 10^{-2}\ \Omega$ cm at room temperature. The thermopower of the samples A, B, and C ($Q < 0.54 \times 10^{22}\ cm^{-3}$) was positive ($150-200\ \mu V\ K^{-1}$) while that of the samples D, E, and F was negative ($-10\ \mu V\ K^{-1}$), indicating changes in the shape of valence band and Fermi energy shift within valence band.[25,27] These results clearly indicate the insulator to metal transition. To further clarify this phenomenon, we measured the temperature dependence of the electrical conductivity (Fig. S6 in the supplementary material) and extracted the activation energy (E_a) of the conductivity around room temperature. The E_a of the electrical conductivity was ~0.2 eV for samples A, B, and C, which is similar to the reported values of $SrFeO_{2.5+x}$ thin films.[28] The E_a for samples A, B, and C is smaller than the bandgap (~2 eV) of $SrFeO_{2.5+x}$ films, indicating that the Fermi energy locates slightly above the valence band maximum. The E_a significantly decreased upon further oxidation and approached zero, confirming that insulator to metal transition occurred.

As shown above, we can see that the optical and electrical properties (insulator to metal) were modulated successfully in all solid-state electrochemical oxidation. The present results clearly show that $SrFeO_x$ has potential as the active material of solid-state multifunctional memory devices.

IV. CONCLUSIONS

In summary, we demonstrated all solid-state electrochemical redox control in the optoelectronic properties of $SrFeO_x$ using the

YSZ substrate as the solid electrolyte. With increasing the degree of oxidation, the phase gradually transfers from $SrFeO_{2.5}$ to $SrFeO_{2.5+x}$ and $SrFeO_{3-x}$. The color of the film changed from yellowish-transparent to dark brown. Although the as-grown $SrFeO_{2.5}$ film showed high resistivity ($\rho > 10^1\,\Omega\,cm$), ρ drastically decreased ($\sim 10^{-2}\,\Omega\,cm$) with increasing the applied charge density. Simultaneously, the thermopower decreased significantly from $\sim +200$ to $\sim -10\,\mu V\,K^{-1}$. The present results would provide a useful design concept for future $SrFeO_x$-based solid-state multifunctional memory devices.

SUPPLEMENTARY MATERIAL

See the supplementary material for the change in the applied current as a function of current application time, x-ray reflectivity, magnified out-of-plane XRD patterns, topographic AFM images, optical transmission spectra, and temperature dependence of the electrical conductivity.

ACKNOWLEDGMENTS

The authors thank T. Ohkura for his experimental help. This research was supported by Grants-in-Aid for Innovative Areas (No. 19H05791) and Scientific Research A (No. 17H01314) from the JSPS. Q.Y. was supported by Grants-in-Aid for JSPS Fellows from the JSPS. A part of this work was also supported by Dynamic Alliance for Open Innovation Bridging Human, Environment, and Materials and by the Network Joint Research Center for Materials and Devices.

DATA AVAILABILITY

The data that support the findings of this study are available from the corresponding author upon reasonable request.

REFERENCES

[1]D. B. Strukov, G. S. Snider, D. R. Stewart, and R. S. Williams, Nature **453**, 80 (2008).
[2]C. S. Hwang and B. Dieny, MRS Bull. **43**, 330 (2018).
[3]M. Kawai, K. Matsumoto, N. Ichikawa, M. Mizumaki, O. Sakata, N. Kawamura, S. Kimura, and Y. Shimakawa, Cryst. Growth Des. **10**, 2044 (2010).
[4]J. D. Ferguson, Y. Kim, L. F. Kourkoutis, A. Vodnick, A. R. Woll, D. A. Muller, and J. D. Brock, Adv. Mater. **23**, 1226 (2011).
[5]H. Jeen, W. S. Choi, M. D. Biegalski, C. M. Folkman, I.-C. Tung, D. D. Fong, J. W. Freeland, D. Shin, H. Ohta, M. F. Chisholm, and H. N. Lee, Nat. Mater. **12**, 1057 (2013).
[6]H. Jeen, W. S. Choi, J. W. Freeland, H. Ohta, C. U. Jung, and H. N. Lee, Adv. Mater. **25**, 3651 (2013).
[7]J.-H. Jang, Y.-M. Kim, Q. He, R. Mishra, L. Qiao, M. D. Biegalski, A. R. Lupini, S. T. Pantelides, S. J. Pennycook, S. V. Kalinin, and A. Y. Borisevich, ACS Nano **11**, 6942 (2017).
[8]A. F. Wells, *Structural Inorganic Chemistry* (Oxford University Press, 2012).
[9]T. Katase, K. Endo, T. Tohei, Y. Ikuhara, and H. Ohta, Adv. Electron. Mater. **1**, 1500063 (2015).
[10]T. Katase, T. Onozato, M. Hirono, T. Mizuno, and H. Ohta, Sci. Rep. **6**, 25819 (2016).
[11]T. Katase, Y. Suzuki, and H. Ohta, Adv. Electron. Mater. **2**, 1600044 (2016).
[12]T. Katase, Y. Suzuki, and H. Ohta, J. Appl. Phys. **122**, 135303 (2017).
[13]H.-Y. Lo, C.-Y. Yang, G.-M. Huang, C.-Y. Huang, J.-Y. Chen, C.-W. Huang, Y.-H. Chu, and W.-W. Wu, Nano Energy **72**, 104683 (2020).
[14]J. J. Tian, H. J. Wu, Z. Fan, Y. Zhang, S. J. Pennycook, D. F. Zheng, Z. W. Tan, H. Z. Guo, P. Yu, X. B. Lu, G. F. Zhou, X. S. Gao, and J.-M. Liu, Adv. Mater. **31**, 1903679 (2019).
[15]Q. Yang, H. J. Cho, H. Jeen, and H. Ohta, Adv. Mater. Interfaces **6**, 1901260 (2019).
[16]Y. W. Long, Y. Kaneko, S. Ishiwata, Y. Tokunaga, T. Matsuda, H. Wadati, Y. Tanaka, S. Shin, Y. Tokura, and Y. Taguchi, Phys. Rev. B **86**, 064436 (2012).
[17]S. Chakraverty, T. Matsuda, H. Wadati, J. Okamoto, Y. Yamasaki, H. Nakao, Y. Murakami, S. Ishiwata, M. Kawasaki, Y. Taguchi, Y. Tokura, and H. Y. Hwang, Phys. Rev. B **88**, 220405 (2013).
[18]A. Maity, R. Dutta, B. Penkala, M. Ceretti, A. Letrouit-Lebranchu, D. Chernyshov, A. Perichon, A. Piovano, A. Bossak, M. Meven, and W. Paulus, J. Phys. D: Appl. Phys. **48**, 504004 (2015).
[19]V. R. Nallagatla, J. Kim, K. Lee, S. C. Chae, C. S. Hwang, and C. U. Jung, ACS Appl. Mater. Interfaces **12**, 41740 (2020).
[20]V. R. Nallagatla and C. U. Jung, Appl. Phys. Lett. **117**, 143503 (2020).
[21]A. Khare, D. Shin, T. S. Yoo, M. Kim, T. D. Kang, J. Lee, S. Roh, I.-H. Jung, J. Hwang, S. W. Kim, T. W. Noh, H. Ohta, and W. S. Choi, Adv. Mater. **29**, 1606566 (2017).
[22]M. S. Saleem, B. Cui, C. Song, Y. Sun, Y. Gu, R. Zhang, M. U. Fayaz, X. Zhou, P. Werner, S. S. P. Parkin, and F. Pan, ACS Appl. Mater. Interfaces **11**, 6581 (2019).
[23]H. Ohta, T. Mizuno, S. Zheng, T. Kato, Y. Ikuhara, K. Abe, H. Kumomi, K. Nomura, and H. Hosono, Adv. Mater. **24**, 740 (2012).
[24]J. Garcia-Barriocanal, A. Rivera-Calzada, M. Varela, Z. Sefrioui, E. Iborra, C. Leon, S. J. Pennycook, and J. Santamaria, Science **321**, 676 (2008).
[25]L. Wang, Z. Yang, M. E. Bowden, and Y. Du, Appl. Phys. Lett. **114**, 231602 (2019).
[26]W. S. Choi, H. Jeen, J. H. Lee, S. S. A. Seo, V. R. Cooper, K. M. Rabe, and H. N. Lee, Phys. Rev. Lett. **111**, 097401 (2013).
[27]V. R. Nallagatla, T. Heisig, C. Baeumer, V. Feyer, M. Jugovac, G. Zamborlini, C. M. Schneider, R. Waser, M. Kim, C. U. Jung, and R. Dittmann, Adv. Mater. **31**, 1903391 (2019).
[28]J. J. Tunney and M. L. Post, J. Electroceram. **5**, 63 (2000).